Limit Cycles from the Similarity Renormalization Group

Alberto Garcia

Department of Physics

The Ohio State University

August 5, 2020

Abstract

The goal of this review is to summarize the results by Niemann and Hammer in detecting and extracting the limit cycle for the $V(r) = \frac{c}{r^2}$ potential [1]. I start by describing why and how this potential is considered to be singular, how the potential strength c contributes to this, and the appearance of Efimov bound-state solutions when solving the Schrödinger equation. In addition, I discuss the regularization and renormalization of the potential and how this leads to a limit cycle. Futhermore, I show how the similarity renormalization group can be used to detect the limit cycle and extract the discrete scaling factor. Finally, I speculate how techniques such as eigenvector continuation and machine learning can be used to detect limit cycles and extract the discrete scaling parameter.

1 Introduction

Quantum chromodynamics (QCD) is a theory that describes the strong interaction between quarks mediated by force-carrier particles known as gluons. Even though QCD can be used in principle to describe the properties of nuclei, we turn to effective field theories (EFT) as a means of choosing more appropriate degrees of freedom. EFT is an approximate but systematically improvable theory used to describe phenomena at an appropriately chosen scale. An example of such a theory is chiral EFT (χEFT), which describes the interactions of nucleons and pions. The attractive nature of χEFT is that it allows one to work with the appropriate degrees of freedom at low energies while maintaining the symmetries of QCD, such as parity and chiral symmetry, by providing a systematic expansion that contains the details of high-energy physics in the form of low-energy constants (LEC) [2].

For χEFT, the pion is a relevant degree of freedom due to its long range interaction. As you approach very low energies, the pion is no longer a long-distance degree of freedom when its mass is larger than the typical deBroglie wavelengths of the nucleons, which allows us to filter the pion contributions into the LEC. At this point, the system can be described by pionless EFT with the degrees of freedom belonging to nucleons. Pionless EFT is used when dealing with nucleon-nucleon (NN) interactions [3]. At very low energies, the physics is dominated by the large scattering lengths, which means pionless EFT also applies to systems such as atomic gases near unitarity. In addition, three-body bound state solutions known as Efimov states are seen in the three-body system when the two-body scattering lengths are large.

In order to keep the low-energy observables invariant when regulating the pionless EFT, the theory must be renormalized. In the process, one finds that there exists a limit cycle. Niemann and Hammer [1] study the singular potential $V(r) = \frac{c}{r^2}$ as a test case in order to understand the behavior of its corresponding limit cycle with hopes of extending their findings to detecting the limit cycle in the pionless EFT for the nuclear three-body system. A more in-depth description of this process is provided in later sections.

There is also motivation for understanding the characteristics of the $\frac{1}{r^2}$ potential because it frequently arises in nature. As an example from molecular physics, consider an electron interacting with a polar molecule such as water. The system can be modeled as an electron-dipole interaction, which has the form of $\frac{1}{r^2}$ [4]. In nuclear physics, this potential serves as a model for EFT three-body interactions for large scattering lengths in the ultraviolet limit since all three particles can be placed on a sphere with hyperradius $\rho^2 = r_{12}^2 + r_{23}^2 + r_{13}^2$ and effective potential $V \propto \frac{1}{\rho^2}$ [5].

In this review, I will outline the work and results in [1] and propose further applications. I start by giving a brief overview on regularization, renormalization, and the similarity renormalization group (SRG). Then, I give a brief description of limit cycles and the different ways they arise in non-relativistic quantum mechanics. In addition, I will discuss the Efimov effect and its connection to the limit cycle. Furthermore, I will talk about the mechanism behind the singular nature of the potential $V(r) = \frac{c}{r^2}$, how to regulate the short-distance physics, and its relevance to SRG. Lastly, I will introduce eigenvector continuation (EC) and machine learning (ML) and their applications to the SRG and limit cycles.

2 Regularization and Renormalization

Regularization is a way of making sense of an ill-defined problem arising from divergences by cutting off the part that corresponds to the divergence and replacing it with a well-defined object known as a regulator or cutoff. In non-relativistic quantum mechanics regularization may be needed if the potential is singular at the origin. This is a type of ultraviolet (UV) divergence and its occurrence is due to short-distance or high-momentum physics. One way of regularizing a UV divergence in coordinate space would involve cutting off the short distance behavior and replacing it with an object such as a square well. In this case, the cutoff will be represented by the width of the well R. The observables, such as binding energies and phase shifts, must be independent of this cutoff in order for the theory to remain invariant.

This is where renormalization comes into play.

The purpose of renormalization is to ensure that the observables have no dependence on the cutoff [6]. In the discussion above, the coupling constant will be the depth V_0 of the square well. The depth now has to change *with* R, acting as a counterbalance to ensure that the underlying physics remains unchanged. We call this a renormalized perturbation theory or effective theory [6]. They measure all the degrees of freedom that we care about, but they do not work for all degrees of freedom that the system can potentially have. In other words, we can make predictions up to the cutoff, but any information beyond that is inaccessible with our current theory.

2.1 The renormalization group

The renormalization group (RG) allows one to study the variations of a system at different scales. The difference between the scales can be thought of as looking at a picture with different resolutions [7]. If we choose to examine a picture of someone's face at low resolutions (low-momenta), we may not be able to make out the fine details, such as the wrinkles. If instead we look at the picture at higher resolutions (high-momenta), we may start seeing the pixels. In other words, the resolution increases (decreases) as we increase (decrease) our scale.

We can apply this thinking to a nucleus. At low-momentum, we may only see the protons and neutrons, but as we increase our resolution (momentum scale) to a high enough threshold, we may start to see interactions between quarks and gluons. Essentially, you choose the appropriate degrees of freedom needed for what you are trying to observe by decoupling low- from high-momentum modes. We cannot learn everything about the system if probed at lower energies, there will be a lack of fine details, but if all we care about are low-energy processes, we can replace the short-distance physics with a model that is simpler without affecting the low-momentum observables. In addition, this simplification is ideal since one can potentially avoid computationally extensive calculations [8]. The specific type

of RG we will be using it discussed in the next section.

3 The similarity renormalization group

The similarity renormalization group (SRG) is used to obtain an effective Hamiltonian by evolving it using flow equations that serve to decouple the low- and high-momentum modes [1]. These flow equations act like a series of infinitesimal transformations controlled by a continuous flow parameter s (units of $1/\text{energy}^2$) that depends on an effective momentum cutoff λ, which serve to slowly and continuously "soften" the interaction [7–9]. We can either drive the Hamiltonian to block diagonal or band diagonal form, as shown in Fig. 1.

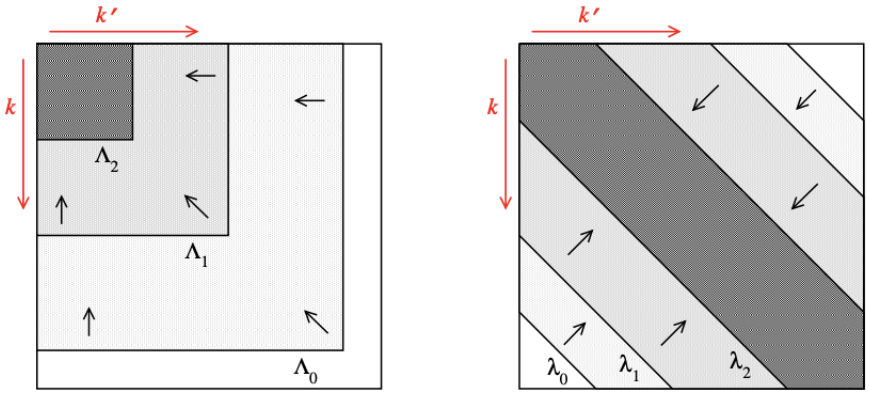

Figure 1: These are two types of SRG transformations. The left image shows the potential matrix being driven to block-diagonal form (with the higher-momentum block being discarded) using a method known as $V_{\text{low k}}$ while the image on the right shows the matrix being driven to band-diagonal form using flow equation evolution. Image taken from Furnstahl [8].

Band-diagonal form decouples momentum modes since the terms that involve a combination of high and low modes come from off-diagonal elements. The off-diagonal elements along the extremes of the matrix (upper right and lower left) involve expectation values with both high and low momenta. With this in mind, we can assert that having these elements go to zero decouple the momenta. Applications of SRG involve treating two- and three-body nucleon-nucleon interactions and are further discussed in [10, 11]. The details of the transformation are discussed in the next section.

3.1 Flow equation for a two-body system

The focus of this section is to give a brief overview of the basic properties of the SRG. We have the following SRG flow equation

$$\frac{dH(s)}{ds} = [[G, H(s)], H(s)] \tag{1}$$

where G is the SRG transformation generator and the square brackets represent commutation. The standard generator used is the kinetic energy T to allow the unitary transformation to drive the Hamiltonian towards band-diagonal form [9]. We will discuss generators in more detail in the next section. The unitary transform of the Hamiltonian is defined as

$$H_s = U_s H U_s^\dagger \equiv T + V_s \tag{2}$$

where the new potential energy operator $V(s) = V_s$ is the evolved interaction and the one-body kinetic energy is independent of the flow parameter. Plugging the evolved Hamiltonian from (2) into the flow equation in (1) we obtain

$$\frac{dH_s}{ds} = 2TV_sT - V_sTT - TTV_s + TV_sV_s - 2V_sTV_s + V_sV_sT. \tag{3}$$

By defining basis states in the space of relative momenta for a two-body interaction and allowing V_s to be a two-body potential we call V_2, 3 can be rewritten as

$$\frac{d}{ds}\langle p|\, V_2\, |q\rangle = -(p^2 - q^2)^2 \langle p|\, V_2\, |q\rangle + \int_0^\infty \frac{d^3k}{(2\pi)^3}\, (p^2 + q^2 - 2k^2) \langle p|\, V_2\, |k\rangle \langle k|\, V_2\, |q\rangle \tag{4}$$

For far off-diagonal elements, the second term in (4) is much smaller than the first term and can be approximately neglected. In this case, the solution to the differential equation is

$$\langle p|\, V_2(s)\, |q\rangle = \langle p|\, V_2(0)\, |q\rangle\, e^{-s(p^2-q^2)^2}. \tag{5}$$

By looking at (5) we see that if the difference of squares between the momenta p and q is large, the exponential term greatly suppresses the corresponding matrix element, thus driving it to zero. This implies that there is indeed a decoupling of the low- and high-momentum modes and the terms that will remain non-zero are the elements along or close to the diagonal where $p \sim q$.

3.2 Generators in SRG

The flow of the SRG equations is defined by the operator G, known as a generator [8]. From expression (5), we can define the effective momentum cutoff as $\lambda \equiv s^{-1/4}$ ($[\lambda] = \text{energy}^{1/2}$). The cutoff λ is analogous to the standard deviation σ of a gaussian, hence gives a good estimate of the width of the band-diagonal in the decoupled Hamiltonian. With this cutoff the start of the evolution $s = 0$ corresponds to $\lambda = \infty$. As the flow parameter is increased, the effective momentum cutoff is lowered. There are alternate generators designed to speed up the evolution process. Two such generators are

$$\begin{aligned} G_e &= \sigma^2 \exp(-T/\sigma^2) \\ G_i &= \frac{\sigma^2}{1 + T/\sigma^2}, \end{aligned} \tag{6}$$

with effective momentum cutoff of $\lambda_a \equiv s^{-1/2}$ obtained the same way as for the standard generator [8]. In fact, these generators, reduce to the standard generator $G = T$ in the small momentum limit when $p \ll \sigma$. Note that the flow equation for these generators *will not* be the same as (5). The nature of (6) allows for decoupling to occur at low energies while the high energy modes are not evolved as much when performing SRG evolutions for small cutoff parameters. Since most of the complexity comes from the high energy modes, the evolution is computationally faster. This is especially important for low-energy nuclear physics, where we mostly deal with physics at low cutoff λ.

4 Limit cycles and their importance

In nonlinear classical mechanics, limit cycles are closed trajectories traced out by a particle in phase space as $t \to \pm\infty$ [12]. In general, a particle with different initial conditions can either spiral towards or away from the previously mapped out trajectory. This leads to three types of limit cycles shown in Fig. 2: stable, unstable, and half-stable.

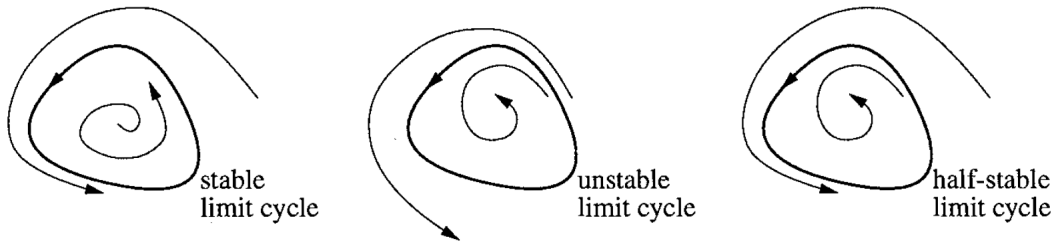

Figure 2: The three different types of limit cycles that can occur. The trajectory are shown by the bolded path. Image taken from Strogatz [13].

The unstable case (repeller) is where the trajectories of the particle near the limit cycle spirals away from it, the stable case (attractor) is when the trajectory spirals towards the limit cycle, and the half-stable case occurs when trajectories spiral both towards and away from the limit cycle. The closed trajectory must be isolated; no other closed trajectory can exist in the neighborhood of the first. If other trajectories are present, they have to either spiral towards or away from the limit cycle [13].

Limit cycles also appear in non-relativistic quantum mechanics for potentials that, under certain conditions, are ill-defined at the origin. In order to obtain unique solutions for the Schrödinger equation, one must regulate the short-distance physics of the potential through the use of a cutoff and apply renormalization to ensure the observables are independent of the cutoff. If only one coupling constant is present, the limit cycle will be one-dimensional and *will not* trace out a path as shown in Fig. 2. Instead, the coupling constant will display tangent-like log-periodic discontinuities in terms of the cutoff (discussed in Sec. 7.1). The limit cycle can be seen as an alternative behavior to the fixed point.

5 The Efimov effect

Efimov showed for a three-body system that if each pair of particles were weakly interacting through short range attractions to the point where they can almost have a two-particle bound state, the three-body system would develop a set of bound state solutions known as Efimov states [14, 15]. Moreover, the three-body bound state spectrum satisfies the relation

$$\frac{E_3^{(n)}}{E_3^{(n+1)}} = \left(e^{\frac{\pi}{s_0}}\right)^2, \tag{7}$$

where $s_0 = 1.00624...$ is the discrete scaling factor. This effect is seen in the unitary limit when the S-wave scattering length is much greater than the range of interaction [16]. The number of three-body bound states depends on two factors: the effective range between each pairs of particles (two-body interactions) and the momentum cutoff. More three-body bound states are produced if the effective range and/or momentum cutoff is increased. Certain potentials with limit cycles display spectrums similar to (7), an example is shown in the next section. These provide an alternative way of calculating the discrete scaling factor.

6 Exploring the $1/r^2$ Potential

Singular potentials can be problematic because they may not have unique solutions in certain regimes. The solutions are not mutually orthogonal or linearly independent, and form an overcomplete system [17]. There are two types of singular potentials: hard and soft. Hard singularities are abrupt, like the delta function potential, while soft singularities continuously develop, like the $1/r^2$ and Coulomb potential. The singular potential $V(r) = \frac{c}{r^2}$, where c is the potential strength, is of particular interest when it comes to limit cycles and Efimov physics because it is known to have an exact limit cycle for certain values of c. In general, limit cycles can only be displayed under two conditions: either two or more coupling constants are present and will appear as a closed loop in coupling constant space, or one coupling

constant is present but with tangent-like log-periodic discontinuities that depends on the cutoff [18]. In our case, we will only have one coupling constant. This potential is also shown to possess a geometric bound-state spectrum analogous to the Efimov effect.

There are many different ways of dealing with this potential in the literature. In coordinate space, the potential can be regulated using a spherical square well potential with short-distance cutoff as shown in [19–21]. Additionally, one can also use a spherical δ-shell potential with an infinitesimally small radius as an alternate regulator [22,23]. In momentum space, a UV cutoff is introduced to regulate the high-momentum modes and renormalization is used to make the observables independent of the imposed cutoff [5, 24].

6.1 Mechanism behind the coupling constant that makes the potential singular

We start with the radial Schrödinger equation, where $u(r) = rR(r)$, with potential $V(r) = \frac{c}{r^2}$ and work in units $\frac{\hbar^2}{2m} = 1$.

$$\frac{d^2u}{dr^2} - \left[\frac{c}{r^2} + \frac{l(l+1)}{r^2} + E\right]u = 0. \tag{8}$$

The singularity in the potential, hence the solution to the differential equation, is located at $r = 0$ so we will turn our attention to the asymptotic behavior of the radial wave function for small r. In this limit, (8) reduces to

$$\frac{d^2u}{dr^2} + \frac{\lambda_c}{r^2}u = 0, \quad \text{where} \quad \lambda_c \equiv -\Big(c + l(l+1)\Big), \tag{9}$$

Focusing on the zero-energy solution with $\ell = 0$, this differential equation can be solved by introducing the ansatz $u = r^\alpha$, where α is to be determined. Following the procedure in

Beane et al. [19], the differential equation takes the polynomial form

$$\frac{\alpha(\alpha-1)r^{\alpha}}{r^2}+\frac{\lambda_c r^{\alpha}}{r^2}=0. \tag{10}$$

We will only look at the case where the solutions to the differential equation are ill-defined (for other solutions refer to the Supplementary material). In solving the resulting polynomial equation we obtain,

$$\alpha_{\pm}=\frac{1}{2}\pm\gamma \quad \text{where} \quad \gamma=\sqrt{\frac{1}{4}+c} \tag{11}$$

and $\lambda_c=-c$. For the case when γ is imaginary, $\gamma=\sqrt{\frac{1}{4}+c}<0$ and the coupling constant is $c<-\frac{1}{4}$. We can write $\gamma=i\sqrt{-\frac{1}{4}-c}$ and define $\gamma\equiv i\nu$. The solution is therefore

$$u(r)=\sqrt{r}\big(Ar^{i\nu}+Br^{-i\nu}\big), \qquad \nu=\sqrt{-c-\frac{1}{4}}. \tag{12}$$

The potential has overcome the centrifugal barrier in this region [4]. After some simplification, the most general solution is

$$R(r)\propto\frac{1}{\sqrt{r}}\cos\big(\nu\ln(kr)+\phi\big), \tag{13}$$

where ϕ is a phase shift. We have inserted a wave number $k=\sqrt{E}$ inside the argument of the natural log to make sure it is unitless. The wave number naturally appears for the general case, where the solutions are modified Bessel functions of the first and second kind. The radial equation describes oscillations whose amplitude increases as $r\to\infty$ causing the phase to be ill-defined at the origin. Looking to see where the wave function is zero, we see that it vanishes for

$$r=\frac{1}{k}\exp\left\{\frac{1}{\nu}\left[\left(n+\frac{1}{2}\right)\pi-\phi\right]\right\}, \tag{14}$$

where n is the principle quantum number. We can interpret this as the wave function having an infinite number of bound states since there is no way to fix ϕ [21, 25, 26]. This is what

makes $V(r) = \frac{c}{r^2}$ singular for $c < -\frac{1}{4}$ and why c is supercritical in this region. We can begin by checking the orthogonality between different states E_a and E_b with solutions u_a and u_b, respectively. Referring back to (8),

$$\frac{d^2u_a}{dr^2} + \left[\frac{\lambda_c}{r^2} - E_a\right]u_a = 0, \quad \frac{d^2u_b}{dr^2} + \left[\frac{\lambda_c}{r^2} - E_b\right]u_b = 0.$$

We multiple each equation by the other's solution and subtract, then integrate over all space. Using integration by parts we obtain

$$\left[u_b\frac{du_a}{dr} - u_a\frac{du_b}{dr}\right]_0^\infty = (E_a - E_b)\int_0^\infty u_a u_b dr \tag{15}$$

In order for the solutions u_a and u_b to orthogonal, the integral on the right-hand side must vanish. For that to be true, the left-hand side of (15) must be equal to zero. We know that the wave function must go to zero when r goes to infinity in order to be normalizable. This leaves the $r = 0$ case, which we can check from the solutions for small r.

A redefinition of the phase in (13) is given by $\phi' = \nu \ln k + \phi$. Letting $u_a(r) = \sqrt{r}\cos\left(\nu\ln(r) + \phi'_a\right)$ and $u_b(r) = \sqrt{r}\cos\left(\nu\ln(r) + \phi'_b\right)$, and plugging these into the left-hand side of (15), we obtain the condition needed to impose orthogonality of the solutions for small r given by

$$\phi'_b - \phi'_a = \nu(\ln k_b - \ln k_a) = n_{ba}\pi, \tag{16}$$

which simplifies to

$$\frac{E_b}{E_a} = \left(e^{\frac{n_{ba}\pi}{\nu}}\right)^2, \tag{17}$$

where $n_{ba} \in (-\infty, 0)$ represents the difference in principle quantum numbers of the energy levels a and b. From (17) we see that there is no lower limit to the energy spectrum and we obtain an accumulation of bound states at the zero energy state. This is analogous to the spectrum produced by Efimov [14, 15, 27]. Case [25] and Schwartz [26] also arrived at this realization, but they concluded that the potential was unphysical if the coupling constant

was in the supercritical regime.

7 SRG and the $1/r^2$ Potential

Instead of attacking the singular potential by solving the Schrödinger equation, we approach the non-uniqueness of the solutions for potential strength in the supercritical regime through EFT. The singularity seen at the origin is considered a UV divergence, which we regulate by imposing a high-momentum (short-distance) cutoff Λ. Using renormalization, a counterterm can be introduced that not only describes the physics at small r, but also makes the low-energy observables independent of Λ [1, 5].

7.1 Renormalizing the $1/r^2$ potential

We apply a Fourier transform to $V(r)$ using the definitions

$$\tilde{V}(Q) = \int_{-\infty}^{\infty} d^3\boldsymbol{r}\, e^{i\boldsymbol{Q}\cdot\boldsymbol{r}}\, V(r), \qquad V(r) = \int_{-\infty}^{\infty} \frac{d^3\boldsymbol{q}}{(2\pi)^3} e^{-i\boldsymbol{Q}\cdot\boldsymbol{r}}\, \tilde{V}(Q). \tag{18}$$

where $Q = |\boldsymbol{p} - \boldsymbol{q}|$ is the momentum transfer.

$$\tilde{V}(Q) = c\int d^3\boldsymbol{r}\, \frac{e^{i\boldsymbol{Q}\cdot\boldsymbol{r}}}{r^2} = 2\pi c \int_0^{\infty} dr \int_0^{\pi} d\theta \sin\theta e^{iQr\cos\theta} = \frac{4\pi c}{Q}\int_0^{\infty} dr \frac{\sin(Qr)}{r} \tag{19}$$

The r integral is known as the Dirichlet integral and has a simple solution of $\pi/2$. The potential $V(r) = \frac{c}{r^2}$ in momentum space is

$$\tilde{V}(Q) = \frac{2\pi^2 c}{Q}. \tag{20}$$

If we only consider S-waves and integrate out the angular dependence, the potential is given by

$$\tilde{V}(p,q) = 2\pi^2 c \left(\frac{\Theta(p-q)}{p} + \frac{\Theta(q-p)}{q}\right) \tag{21}$$

where Θ denotes the Heaviside step function, and q and p are the incoming and outgoing momenta, respectively. The overall goal is to be able to calculate low-energy observables, such as the bound state spectrum and scattering phase shifts. To do this we introduce the Lippmann-Schwinger integral equation in the center-of-mass frame

$$t_E(\boldsymbol{p},\boldsymbol{p}') = \tilde{V}(\boldsymbol{p},\boldsymbol{p}') + \int \frac{d^3q}{(2\pi)^3} \frac{t_E(\boldsymbol{q},\boldsymbol{p}')}{E - q^2 + i\epsilon}\, \tilde{V}(\boldsymbol{q},\boldsymbol{p}), \tag{22}$$

where $E = k^2$ is the total energy and $t_E(\boldsymbol{q},\boldsymbol{p}')$ is the partial wave T-matrix. If we expand in partial-waves and integrate over the relative angle between $\boldsymbol{p}$ and $\boldsymbol{p}'$ we obtain

$$t_E(p,k) = \tilde{V}(p,k) + \frac{1}{2\pi^2}\int_0^\infty \frac{dq\; q^2}{E - q^2 + i\epsilon}\, t_E(q,k)\tilde{V}(p,q), \tag{23}$$

To relate (23) to the phase shifts it must be evaluated on-shell, meaning $E = k^2$ and $k = p' = p$. The phase shifts δ are given by

$$k\cot\delta = ik - \frac{4\pi}{t_E(k,k)|_{E=k^2}}. \tag{24}$$

We now focus our attention on the integral term of (23). For the zero-energy bound state solution we obtain

$$\phi_0(p) = -c\bigg[\int_0^p dq \frac{\phi_0(q)}{p} + \int_p^\infty dq \frac{\phi_0(q)}{q}\bigg)\bigg]. \tag{25}$$

This equation is known as a Voltera integral equation of the first kind. We try the ansatz $\phi_0(p) = p^\alpha$. Taking the derivative of the integral equation in terms of p,

$$\alpha p^{\alpha-1} = c\int_0^p dq \frac{q^\alpha}{p^2} \quad \longrightarrow \quad \alpha(\alpha+1) - c = 0.$$

The polynomial equation for α gives us the same conditions, the same solutions for the wave function, and the same non-uniqueness for $c < -1/4$ as in Sec. 6.1. We restate the results

$$R(r) \propto \frac{1}{\sqrt{r}} \cos\big(\nu \ln(kr) + \phi\big), \qquad \nu = \sqrt{-c - \frac{1}{4}}. \tag{26}$$

Instead, we turn to renormalization. We regularize the Lippmann-Schwinger equation using a hard momentum cutoff Λ for high momenta and introduce a counterterm $\delta V(\Lambda) = 2\pi^2 c\, \frac{H(\Lambda)}{\Lambda}$ for the potential

$$V = V(q) + \delta V(\Lambda) \quad \longrightarrow \quad V(q,\Lambda) = 2\pi^2 c \left(\frac{\Theta(p-q)}{p} + \frac{\Theta(q-p)}{q} + \frac{H(\Lambda)}{\Lambda} \right). \tag{27}$$

Plugging this into the Lippmann-Schwinger equation and introducing the cutoff

$$t_E(p,k) = 2\pi^2 c \left[f(p,k) + \frac{H(\Lambda)}{\Lambda} \right] + c \int_0^\Lambda \frac{dq\; q^2}{E - q^2 + i\epsilon} \left[f(p,q) + \frac{H(\Lambda)}{\Lambda} \right] t_E(q,k), \tag{28}$$

where

$$f(p,q) = \frac{\Theta(p-q)}{p} + \frac{\Theta(q-p)}{q}. \tag{29}$$

Focusing on the integral equation, we look for the zero-energy bound state solution

$$\phi_0(p) = -c \int_0^\Lambda dq \left[f(p,q) + \frac{H(\Lambda)}{\Lambda} \right] \phi_0(q), \tag{30}$$

We can determine the coupling constant $H(\Lambda)$ by imposing the condition that varying the cutoff parameter should not change the observables. By taking the derivative of (30) in terms of the cutoff Λ and solving the resulting differential equation, we obtain

$$H(\Lambda) = \frac{1 - 2\nu \tan(\nu \ln(\Lambda/\Lambda_*))}{1 + 2\nu \tan(\nu \ln(\Lambda/\Lambda_*))}, \tag{31}$$

where Λ_* is a free parameter used to fix the relative phase ϕ.

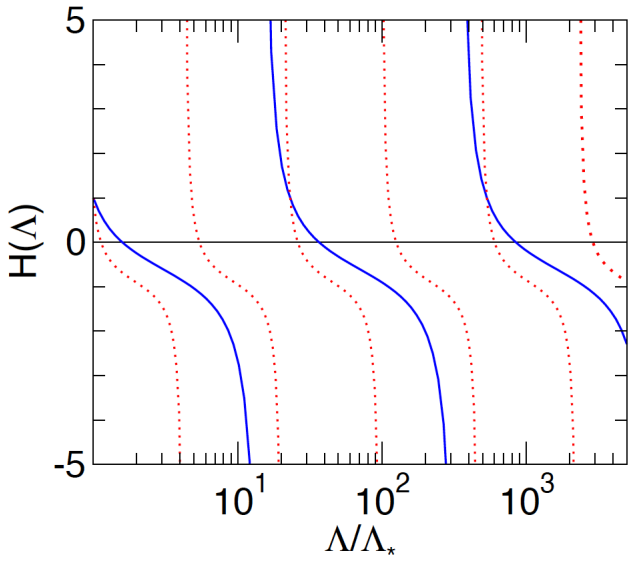

Figure 3: The dimensionless coupling constant $H(\Lambda)$ for $\nu = 1$ (solid blue) and $\nu = 2$ (dashed red). We hold the least bound-state energy fixed. Image taken from Hammer [5].

From Fig. 3 we can see that there is periodicity present in the dimensionless coupling constant $H(\Lambda)$ introduced by the tangent terms. Looking at (31), we can determine the periodic factor by setting the tangent term in the numerator equal to zero

$$\tan(\nu \ln(\Lambda/\Lambda_*)) = 0 \quad \longrightarrow \quad \Lambda = \Lambda_* e^{n\pi/\nu}. \tag{32}$$

This relation is similar to the bound state spectrum calculated in (17). Restating the results,

$$\frac{E^{(n)}}{E^{(n+1)}} = e^{2\pi/\nu}. \tag{33}$$

If we allow the coupling constant to vary with the cutoff parameter, the binding energies become independent of the cutoff.

$$\frac{\Lambda}{\Lambda_*} = \big(\lambda_0\big)^n \quad \longrightarrow \quad \lambda_0 = e^{\pi/\nu} \tag{34}$$

We also see that when Λ is increased by a power of the preferred scaling factor λ_0, new bound states will appears. There is still an accumulation of bound states at zero energy, but

the energy is now constant when we allow the coupling constant to vary with Λ. Regulating and renormalizing the potential does not change the accumulation of bound states, instead it ensures that the bound state energy is constant and saturates at some lower bound $\propto \Lambda^2$ [5]. The problem is now well-defined.

The connection between the energy spectrum (33) and the log-periodicity of the coupling constant is useful because it allows us to study properties of the limit cycle and how it changes by varying the bound state spectrum of the system through the parameter ν. Hammer [28] further extends this treatment by including a long-range attractive Coulomb potential.

7.2 Limit cycle and the SRG

The process of renormalizing $V(r) = \frac{c}{r^2}$ has shown that the regulated potential displays a limit cycle, the observables are independent of the cutoff, and the energy separation is dependent on a preferred scaling factor. The potential can be evolved using SRG as an attempt to detect the limit cycle by looking for periodic oscillations in the matrix elements. In essence, the running of the the cutoff in Fig. 3 is like running λ in the SRG evolution. The coupling constant will have some periodicity as you change the cutoff. By definition, all observables will remain constant throughout the evolution [1]. All dimensionful quantities are given in units of a free length scale l_0.

Niemann [1] shows that the limit cycle can be seen when producing heat maps pertaining to the evolution of $V(r)$ in the supercritical regime for the standard and alternate generators. Starting with the standard generator at fixed λ, the emergence of separate positive and negative regions along the diagonal of the heat map can be seen in Fig. 4 as the potential strength is taken from the subcritical regime, where there is no limit cycle, to the supercritical regime, where we have shown one exists. In the subcritical regime, $c > -1/4$, the evolution shows a smooth trend towards zero as λ is lowered. As the potential strength is increased to the critical value $c = -1/4$, the matrix elements show small oscillations between positive and negative values at the onset of the evolution. Once the potential strength is in the

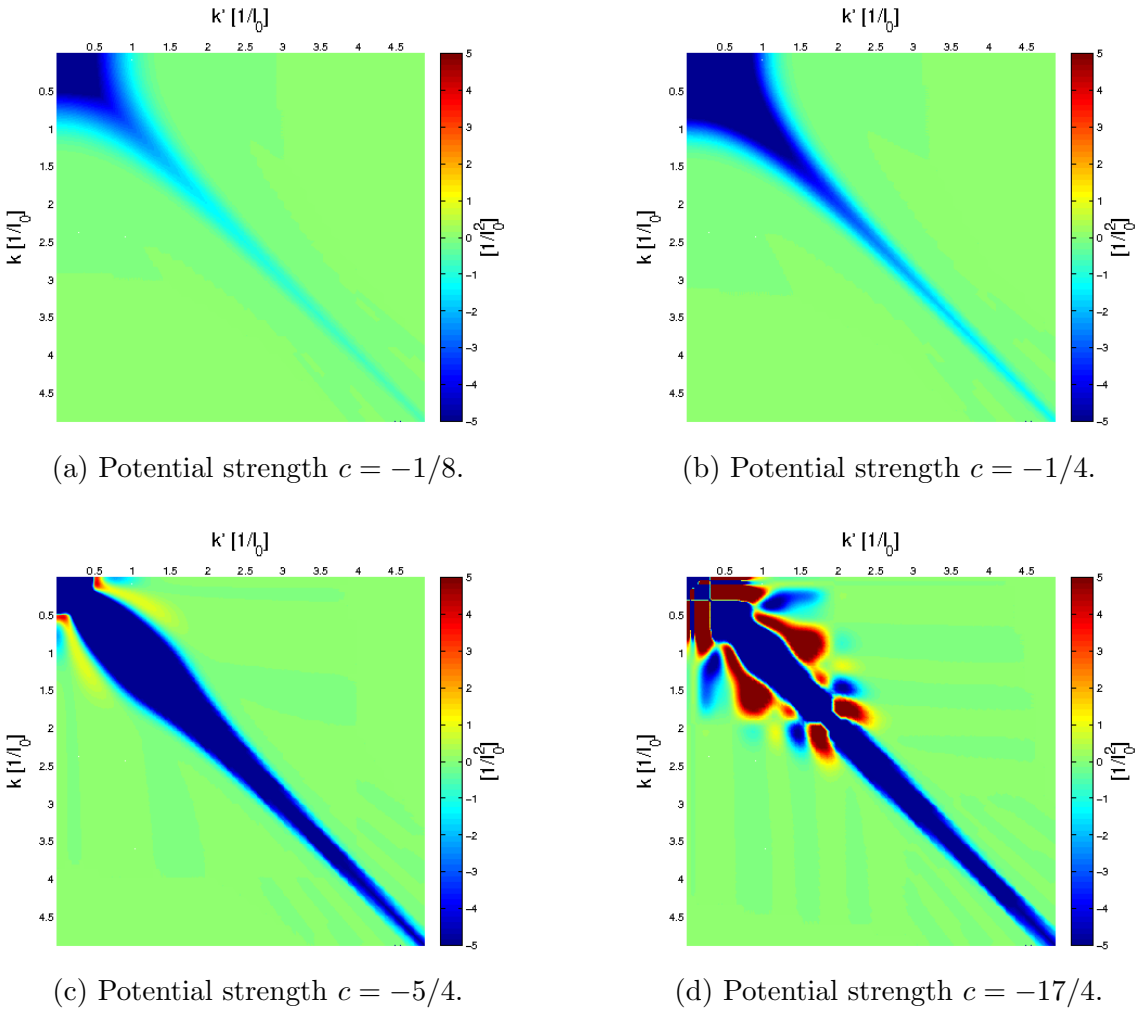

(a) Potential strength $c = -1/8$.

(b) Potential strength $c = -1/4$.

(c) Potential strength $c = -5/4$.

(d) Potential strength $c = -17/4$.

Figure 4: SRG evolution of $V(r) = \frac{c}{r^2}$ for the standard generator $G = T$. Parameters: initial UV cutoff $\Lambda = 20\ l_0^{-1}$, evolved to $\lambda = 1\ l_0^{-1}$. All the parameters excluding c are kept constant. Image taken from Niemann [1].

supercritical regime, $c < -1/4$, the oscillations have noticeably increased in frequency. As c decreases ν increases, leading to an increase in oscillations related to the scaling factor $e^{\pi/\nu}$. In addition, the appearance of positive and negative regions in the supercritical regime, $c < -1/4$, confirms their relation to the limit cycle. As a note, the described behavior occurs on a logarithmic scale for the flow parameter s. The results presented in the supercritical regime will now be quoted in terms of ν: $c < -1/4 \to \nu > 0$

Fig. 5 shows the evolution of the potential in the supercritical regime, $\nu > 0$, using the alternate generators shown in (6). Oscillations between positive and negative matrix elements

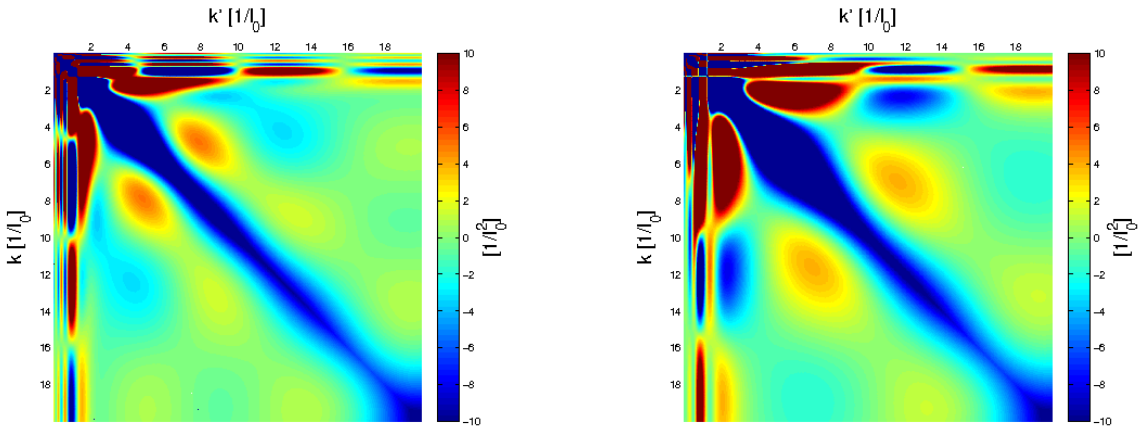

(a) Evolved to $\lambda_a \approx 8.35\ l_0^{-1}$ for G_e.

(b) Evolved to $\lambda_a \approx 10.75\ l_0^{-1}$ for G_i.

Figure 5: SRG evolution of $V(r) = \frac{c}{r^2}$ using the alternate generators, (6). Parameters: $\nu = 9$, initial UV cutoff $\Lambda = 20\ l_0^{-1}$, $\sigma = 2\ l_0^{-1}$. Image taken from Niemann [1].

are also present, but they have different signatures compared to the standard generator. They are no longer purely along the diagonal, but are also found compressed along the edges of the heat map. These characteristics are due to the structure of the generators. As discussed in Sec. 3.2, these generators reduce to the standard generator for momenta much smaller than the cutoff parameter, $p \ll \sigma$. For this reason, the oscillations are only seen in regions involving $k(k')$ values smaller than σ. In addition, these generators decouple the momenta at low energies and hardly evolve the high momentum modes, accounting for the matrix elements corresponding to the high momenta being at or around zero. Using alternate generators also confirms the existence of the limit cycle. Now that we have been able to detect them, extract the discrete scaling factor from the evolved potential in the next section.

7.3 Extracting the discrete scaling factor

The discrete scaling factor is an attribute of the limit cycles that is of great interest. This scaling factor determines the periodic nature of the limit cycle since the coupling constants introduced through renormalization in the form of counterterms will return to their initial

values when the cutoff is changed by the scaling factor. As such, limit cycles must be scale-invariant under discrete transformations [18].

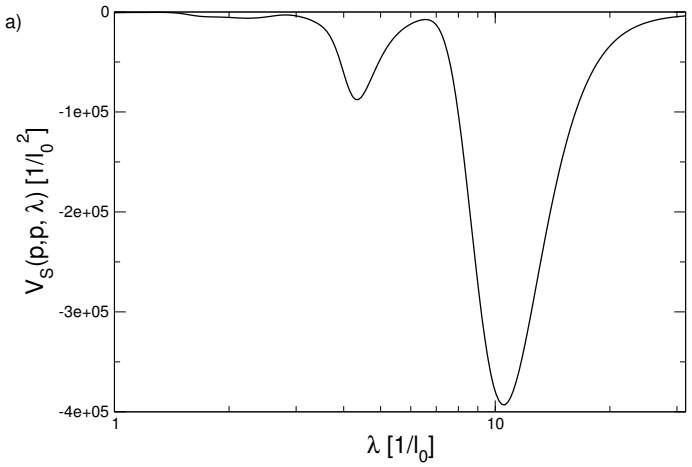

Figure 6: Diagonal matrix elements of the evolved potential for variable effective cutoff momenta using the standard generator. Parameters: $\nu = 9$, $\Lambda = 20\ l_0^{-1}$, $p \approx 0.84\ l_0^{-1}$. Image taken from Niemann [1].

Niemann proposed measuring this scaling factor by examining the diagonal matrix elements of the evolved potential. Since the purpose of the evolution is to cause all terms away from the diagonal to approach zero while the diagonal remains intact, we can conclude that the limit cycle must be the most distinguishable along the diagonal. Fig. 6 shows an arbitrary diagonal matrix element of the evolved potential with varying λ using the standard generator on a log-log plot. The oscillations of the matrix element with varying cutoff indicate the existance of a limit cycle. As can be seen, there is hardly any oscillations. With no clear period, the scaling factor cannot be extracted. Instead, we examine the potentials evolved using the alternate generators.

In Fig. 7, structured oscillations can clearly be seen for the diagonal matrix elements of the potential evolved using the alternate generators. Before we begin discussing the extraction of the discrete scaling factor, we need to determine if the oscillations have any dependence on the width factor σ from Sec. 3.2 to ensure we are looking in the correct regime. Looking back to Sec. 3 on the discussion of the alternate generators, we can reason that for momenta greater than σ, there will be no oscillations present. The reason stems from the generators

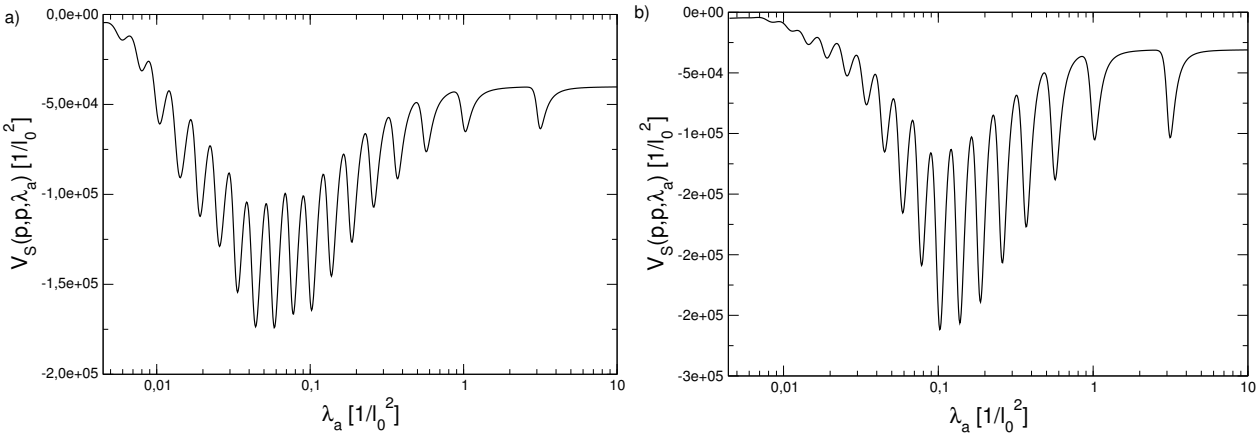

(a) Exponential generator with $p = 1.19\ l_0^{-1}$.

(b) Inverse generator with $p = 1.55\ l_0^{-1}$.

Figure 7: Diagonal matrix elements of the evolved potential for variable effective cutoff momenta using the alternate generators. Parameters: $\nu = 11$, cutoff $\Lambda = 30\ l_0^{-1}$, $\sigma = 0.05\ l_0^{-1}$. Image taken from Niemann [1].

mostly ignoring the higher momentum modes. If the momentum is smaller than σ, the number of oscillations will decrease. This comes from the alternate generators reducing to the standard generator for small momentum p. Hence, the best place to look is for $p \approx \sigma$. Fig. 8 shows the diagonal elements of the potential evolved with the inverse generator for multiple values of momentum. Judging from the graphs, oscillations are more apparent when $p \approx \sigma$ as proposed above. As the momentum is increased, the graph begins to smooth out and the oscillations disappear. If the momentum is chosen to be smaller than σ, the number of oscillations start decreasing. We conclude that there is a strong dependence between the number of oscillations and the values chosen for p and σ.

Looking back at Fig. 7, the discrete scaling factor (See (32) in Sec. 7.1) for the evolved potential obtained from the exponential generator with $\nu = 11$ and $\nu = 5$ is analytically calculated to be

$$\frac{\Lambda}{\Lambda_*} = e^{\pi/11} \approx 1.33, \qquad \frac{\Lambda}{\Lambda_*} = e^{\pi/5} \approx 1.87. \tag{35}$$

The period of oscillation can be extracted from the figures by taking ratios of the effective momentum cutoff corresponding to the maxima and minima of the oscillations. We only

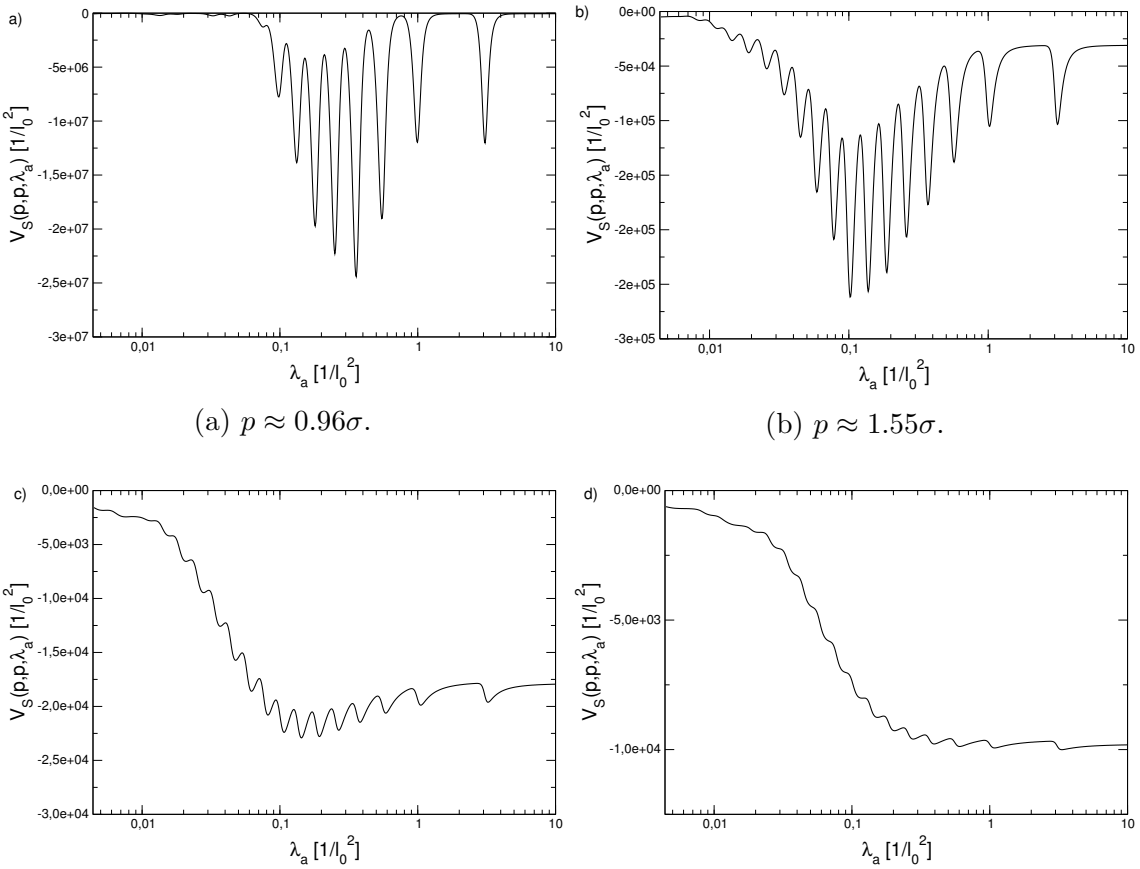

(a) $p \approx 0.96\sigma$. (b) $p \approx 1.55\sigma$.

(c) $p \approx 2.68\sigma$. (d) $p \approx 4.88\sigma$.

Figure 8: Diagonal matrix elements of the evolved potential for variable effective cutoff momenta using the inverse generator. Parameters: $\nu = 11$, cutoff $\Lambda = 30\ l_0^{-1}$, $\sigma = 0.05\ l_0^{-1}$. Image taken from Niemann [1].

show a graph for the case where $\nu = 11$. A summary of Niemann's findings is given in Fig. 9 for $\nu = 11$ and $\nu = 5$.

As can be seen, the ratios of maxima and minima give an accurate result for both discrete scaling factors. The initial oscillations are transient resulting in an inaccurate value for the discrete scaling factor. This is most likely due to finite cutoff effects, but as the evolution process is continued, the oscillations start to stabilize and become more periodic. The scaling factors extracted in this region are within 5% of the theoretical value.

oscillation	$\nu = 11$		$\nu = 5$	
	maxima	minima	maxima	minima
1	2.94	3.08	3.26	3.36
2	1.76	1.80	2.11	2.11
3	1.52	1.54	1.91	1.91
4	1.42	1.43	1.87	1.85
5	1.38	1.39	1.83	1.81
6	1.36	1.36	1.85	1.80
7	1.35	1.34	1.84	1.79
8	1.31	1.32		1.78
9	1.33	1.33		
10	1.34	1.33		
11	1.30	1.31		
12	1.33	1.31		
13	1.34	1.34		
14	1.38	1.35		
15	1.36	1.36		
16	1.33	1.31		
17		1.34		

Figure 9: Extracted ratios of effective momentum cutoff parameter for $\nu = 11$ and $\nu = 5$ pertaining to the maxima and minima values of the oscillations seen along the diagonal of the evolved potential. The exponential generator was used for the evolution process. Parameters: $\Lambda = 30\ l_0^{-1}$, $\sigma = 0.05\ l_0^{-1}$, $p \approx 1.19\sigma$. Table taken from Niemann [1].

8 Applications

In this section, we discuss further applications that can be used to detect limit cycles and extract discrete scaling factors.

8.1 SRG and Eigenvector Continuation

Eigenvector continuation (EC) is a technique that relies on solutions to a Hamiltonian for several sets of known parameters to formulate a basis. Using this basis, we can accurately interpolate and extrapolate solutions for the same Hamiltonian with different parameters [29]. A simple example is scattering in a square well. We take previously known phase shifts for a specified scattering energy and build a basis with their corresponding wave functions. Each wave function has a weight attached to it that is calculated using EC. With this basis in hand, we can extrapolate and interpolate to unknown phase shifts and wave functions.

EC can be applied to the SRG transformation problem for varying cutoffs λ. I briefly outline the methodology:

1. Pick an initial starting flow/cutoff parameter.

2. Start the SRG evolution process for the potential in question, being sure to record the soften potential at different cutoff parameters.

3. Build the effective Hamiltonian for each cutoff parameter previously chosen.

4. Using these effective Hamiltonians, the eigenvectors for each corresponding λ can be calculated by solving the Schrödinger equation at a specified energy or for the bound states.

5. Apply EC using the previously chosen cutoffs and their eigenvectors to calculate their corresponding weights and formulate a basis.

6. Use the new basis to extrapolate/interpolate for any value of λ.

An especially interesting application would be to apply EC to chiral perturbation theory for varying λs and extrapolate to very small λ. What this implies is that we start with a theory that contains pions and extrapolate to pionless EFT. This may allow us to detect signatures of the limit cycle in pionless EFT in an analogous manner to what Niemann did, by looking at a three-body system (like the triton).

8.2 Detecting Limit Cycles with Machine Learning

Machine learning can be used to extract discrete scaling factor using convolutional neural networks (CNN). CNNs are neural networks that mostly deal with image recognition. They work by assigning weights and biases to important features in images and uses what it has learned to differentiate between other images. The process of extracting scaling factor can be done by producing images of the SRG evolution and classifying oscillations by the maxima (or minima) using image classification methods. A model can be built to recognize the maxima/minima of the SRG heat map and relate these back to the effective momentum cutoff parameters λ. Then the same process of taking the ratios of the corresponding effective

momentum cutoff parameters can be done to calculate the scaling factor. In addition, one can train a CNN to predict the scaling factor from heat maps produced by an evolved potential with an unknown generator. This would involve training the CNN to predict the scaling factor for heat maps where the generator and parameter is known and extrapolating to unknown results.

9 Conclusion

We have shown that the solutions to the Schrödinger equation for the potential $V(r) = \frac{c}{r^2}$ exhibits a spectrum of bound states analogous to the Efimov effect due to the solutions being non-unique when the potential strength c is in the supercritical regime. Using regularization and renormalization, we can fix the issue of non-uniqueness through the use of a counterterm that accounts for the unknown short-distance physics found at the singularity and keeps the low-energy observables fixed. This regulated singular potential will now display a limit cycle as the cutoff is varied, causing the coupling constant to be log-periodic in the cutoff. This periodicity will be determined by a preferred scaling factor, which is related to the potential strength. We then show that it is possible to extract the discrete scaling factor by evolving a potential that contains a limit cycle using the SRG. We extend the application of detecting limit cycles with the SRG by suggesting using EC on a chiral EFT nuclear three-body system with the goal of extrapolating to pionless EFT in order to detect its limit cycle. In addition, a method of extracting and predicting the discrete scaling factor using CNNs is proposed.

10 Supplementary

Restating the differential equation

$$\frac{\alpha(\alpha-1)r^{\alpha}}{r^2}+\frac{\lambda_c r^{\alpha}}{r^2}=0.$$

Solving for the real roots of the polynomial and plugging them into the ansatz, the solution to the differential equation is

$$u(r)=Ar^{\frac{1}{2}+\gamma}+Br^{\frac{1}{2}-\gamma}, \qquad \gamma=\sqrt{\frac{1}{4}-\lambda_c}. \tag{36}$$

We know that $\lambda_c=-c$, therefore, $\gamma=\sqrt{\frac{1}{4}+c}$. We must now understand the behavior of the solution for different values of γ (the case where $\gamma<0$ is discussed in Sec. 6). For nonzero γ we impose the condition $\gamma=\sqrt{\frac{1}{4}+c}>0$, which tells us $c>-\frac{1}{4}$. We can determine if the solution is unique by taking the Wronskian of the solutions

$$\mathcal{W}(y_1,y_2)=\begin{vmatrix} r^{\frac{1}{2}+\gamma} & r^{\frac{1}{2}-\gamma} \\ (\frac{1}{2}+\gamma)r^{\gamma-\frac{1}{2}} & (\frac{1}{2}-\gamma)r^{-\gamma-\frac{1}{2}} \end{vmatrix}=-2\gamma\neq 0. \tag{37}$$

We see that we obtained two linearly independent solutions, the potential is well behaved, and the general solution to the Schrödinger equation is unique. The coupling constant for values $c>-\frac{1}{4}$ is subcritical. For a repulsive potential, $c>0$, the problem is straightforward and the solutions are perfectly acceptable. The same can be said for an attractive potential, $c<0$, provided that $c>-\frac{1}{4}$. For the case when $\gamma=0$, the coupling constant is $c=-\frac{1}{4}$. The solution is given by

$$u(r)=A'\sqrt{r}, \tag{38}$$

As opposed to the previous case where we obtained two linearly independent solutions, we only ended up with one solution. In this case, the coupling constant when $c=-\frac{1}{4}$ is critical.

Acknowledgements

I would like to thank my committee for their time and support throughout the candidacy exam. I would especially like to thank Prof. Dick Furnstahl for his patience and invaluable time spent answering questions and provide feedback on this paper. I would also like to thank my research group for helping me prepare for the candidacy exam by attending my practice talks, asking questions that helped me understand the paper at a deeper level, and for meeting with me to discuss concepts I did not fully comprehend. Finally, I would like to thank Yonas Getachew for proof-reading this paper.

References

[1] P. Niemann and H. W. Hammer. Limit Cycles from the Similarity Renormalization Group. *Few-Body Systems*, 56(11):869–879, May 2015.

[2] E. Epelbaum. Nuclear forces from chiral effective field theories. *arXiv:1001.3229v1 [nucl-th]*, Jan. 2010.

[3] E. Epelbaum, H.-W. Hammer, and U.-G. Meißner. Modern Theory of Nuclear Forces. *arXiv:0811.1338v1 [nucl-th]*, Nov. 2008.

[4] S. A. Coon and B. R. Holstein. Anomalies in Quantum Mechanics: the $1/r^2$ Potential. *arXiv:0202091v1 [quant-ph]*, Feb. 2002.

[5] H.-W. Hammer and B. G. Swingle. On the limit cycle for the $1/r^2$ potential in momentum space. *Annals Phys.*, 321:306–317, Apr. 2005.

[6] M.E. Peskin and D.V. Schroeder. *An Introduction to Quantum Field Theory*. Westview Press, 1st edition, Oct. 1995.

[7] E. Jurgenson. *Applications of the Similarity Renormalization Group to the Nuclear Interaction*. PhD thesis, The Ohio State University, 2009.

[8] R. J. Furnstahl. The Renormalization Group in Nuclear Physics. *Nucl. Phys. B*, 228:139–175, Jul. 2012.

[9] S. K. Bogner, R. J. Furnstahl, and R. J. Perry. Similarity renormalization group for nucleon-nucleon interactions. *Phys. Rev. C*, 75:061001, Jun 2007.

[10] S. Szpigel and R. J. Perry. The Similarity Renormalization Group. *Quantum Field Theory, A 20th Century Profile*, 2000.

[11] S. K. Bogner, R. J. Furnstahl, and R. J. Perry. Three-body forces produced by a similarity renormalization group transformation in a simple model. *Annals Phys.*, 323:1478–1501, Jun. 2008.

[12] K. Hellevik and O. T. Gudmestad. Limit cycle oscillations at resonances. *IOP Conference Series: Materials Science and Engineering*, 276:012020, Dec. 2017.

[13] S. H. Strogatz. *Nonlinear Dynamics and Chaos: With Applications to Physics, Biology, Chemistry, and Engineering*. CRC Press, 1st edition, Dec. 2000.

[14] V. Efimov. Energy levels arising form the resonant two-body forces in a three-body system. *Phys. Lett. B*, 33:563–564, Dec. 1970.

[15] V. N. Efimov. Weakly Bound States Of Three Resonantly Interacting Particles. *Yadern. Fiz. 12: 1080-91*, Nov. 1970.

[16] H.-W. Hammer and L. Platter. Efimov states in nuclear and particle physics. *Annual Review of Nuclear and Particle Science*, 60(1):207–236, Nov. 2010.

[17] T. Fülöp. Singular Potentials in Quantum Mechanics and Ambiguity in the Self-Adjoint Hamiltonian. *SIGMA*, 3, Nov. 2007.

[18] H.-W. Hammer and L. Platter. Efimov physics from a renormalization group perspective. *Phil. Trans. of the Royal Soc. A*, Jul. 2011.

[19] S. R. Beane, P. F. Bedaque, L. Childress, A. Kryjevski, J. McGuire, and U. van Kolck. Singular potentials and limit cycles. *Phys. Rev. A*, 64:042103, Sep. 2001.

[20] M. Bawin and S. A. Coon. Singular inverse square potential, limit cycles, and self-adjoint extensions. *Phys. Rev. A*, 67:042712, Apr. 2003.

[21] S. Gopalakrishnan and W. A. Loinaz. *Self-Adjointness and the Renormalization of Singular Potentials*. PhD thesis, Amherst College, Apr. 2006.

[22] E. Braaten and D. Phillips. Renormalization-group limit cycle for the $1/r^2$ potential. *Phys. Rev. A*, 70:052111, Nov. 2004.

[23] D. Bouaziz and M. Bawin. Singular inverse-square potential: Renormalization and self-adjoint extensions for medium to weak coupling. *Phys. Rev. A*, 89:022113, Feb. 2014.

[24] E. J. Mueller and T.-L. Ho. Renormalization Group Limit Cycles in Quantum Mechanical Problems. *arXiv:0403283 [cond-mat.stat-mech]*, Mar. 2004.

[25] K. M. Case. Singular Potentials. *Phys. Rev.*, 80(5):797–806, Dec. 1950.

[26] C. Schwartz. Almost singular potentials. *Journal of Mathematical Physics*, 17(6):863–867, Jun. 1976.

[27] P. Naidon and S. Endo. Efimov physics: a review. *Reports on Progress in Physics*, 80(5):056001, Mar. 2017.

[28] H.-W. Hammer and R. Higa. A model study of discrete scale invariance and long-range interactions. *The European Physical Journal A*, 37(2):193–200, 2008.

[29] R. J. Furnstahl, A. J. Garcia, P. J. Millican, and X. Zhang. Efficient emulators for scattering using eigenvector continuation. *arXiv:2007.03635v2 [nucl-th]*, Jul. 2020.